Colloids and Surfaces B: Biointerfaces xxx (xxxx) xxxx

Contents lists available at ScienceDirect

Colloids and Surfaces B: Biointerfaces

journal homepage: www.elsevier.com/locate/colsurfb

An analytical method to control the surface density and stability of DNA-gold nanoparticles for an optimized biosensor

Stephanie Hwu, Manon Garzuel, Csaba Forró, Stephan J. Ihle, Andreas M. Reichmuth, Fiodar Kurdzesau, János Vörös*

Laboratory of Biosensors and Bioelectronics, Institute for Biomedical Engineering, ETH Zurich, 8092, Zurich, Switzerland

ARTICLE INFO

Keywords:
DNA functionalization
Gold nanoparticle
Colloid stability
Quantifying ligand density
Snap freezing
Multifunctional colloids

ABSTRACT

DNA functionalized gold nanoparticles (DNA-AuNPs) have shown great potential for biosensing as they combine the excellent optical properties of gold nanoparticles and the molecular recognition function of DNA. Since the DNA density determines the assay performance and the stability of the conjugate, a precise control of the surface density of DNA-AuNP is crucial for an optimized biosensor. Here we report a simple assay for quantifying multiple unlabeled DNAs on AuNPs. The assay relies on potassium cyanide (KCN) to first dissolve the AuNPs, which then releases surface bound DNA for quantification through a double-stranded DNA dye. Using this analytical quantification method, we investigated several strategies to control the surface density of DNA-AuNPs. Besides the precise control of DNA density, the stability of DNA-AuNPs after conjugation is also important in developing a biosensor with optimal performance. Without proper storing conditions, DNA-AuNPs are unstable and aggregate over time. To overcome this problem, we developed a long-term storage solution to ensure the stability and quality of DNA-AuNPs after conjugation which would benefit any DNA-AuNP-based biosensor.

1. Introduction

Gold nanoparticles (AuNPs) are popular in the fields of biomedicine such as biosensing [1,2], imaging [3,4] and drug delivery systems [5,6]. AuNPs are particularly suitable for diagnostics as they can be conveniently modified with thiolated ligands to detect specific molecules of interest [7,8]. One example of such a molecule is microRNA (miRNA), an endogenous RNA, the dysregulation of which is related to the progression of many human diseases such as cancer [9,10]. In the case of nucleic acid detection, including miRNA, AuNPs are usually functionalized with thiolated probe DNA (DNA-AuNPs). The molecular recognition ability of DNA allied with the unique optical properties of AuNPs makes DNA-AuNPs ideal materials for miRNA sensing [11,12].

The surface density of DNA-AuNPs determines the performance of DNA-AuNP-based sensors [13,14]. At low surface densities, the probe DNA non-specifically interacts with the AuNP surface which limits the hybridization of DNA-AuNP with the target molecule [15,16]. Such low probe DNA densities also result in irreversible aggregation of DNA-AuNPs as the repulsion between DNA strands is insufficient to keep the particles apart in solution [17]. At high surface densities, the probe DNA strands are oriented upright, and the steric hindrance and electrostatic repulsion allow the particles to remain stable even in high ionic strength solutions. However, the electrostatic force also repels the negatively charged target [17], which can decrease the hybridization efficiency [15,16], and too high surface densities can even eliminate the hybridization capability of the capture probes [18].

While the stability of DNA-AuNPs can be improved by increasing the probe DNA density, its stability over time is difficult to control and often leads to reproducibility issues. There are several explanations for this problem. For example, the aggregation of DNA-AuNPs due to non-specific interaction between the probe DNA, sedimentation of DNA-AuNPs and contamination with enzymes such as DNase and RNase during storage all lead to stability issues when stored in solution. The most common approach to conjugate DNA-AuNPs involves several salt addition steps which take more than 12 h to incrementally attach thiolated DNA to the AuNP surface [19]. Without proper storage, the stability of DNA-AuNPs decreases over time and the cumbersome preparation needs to be repeated on a regular basis to ensure the quality of DNA-AuNPs.

Since hybridization efficiency and particle stability dictate performance, an analytical quantification method and precise control of the surface density are important for DNA-AuNP-based sensors. Several approaches to quantify DNA on AuNPs have been developed in the past and they can be categorized into (1) quantification of fluorescently

* Corresponding author.
E-mail address: janos.voros@biomed.ee.ethz.ch (J. Vörös).

https://doi.org/10.1016/j.colsurfb.2019.110650
Received 13 September 2019; Received in revised form 15 November 2019; Accepted 16 November 2019

labeled [15,20–22] and (2) unlabeled DNA on AuNPs [23,24]. In the case of measuring *labeled* DNA, fluorescent DNA is first immobilized on the AuNPs, and the fluorescence intensity of the labeled DNA is measured after its displacement from the surface [15]. The method is sensitive but it faces several challenges. For example, in the case of multifunctional DNA-AuNP (*e.g.* AuNPs conjugated with different DNA sequences), different spectrally non-overlapping dyes are required to quantify multiple sequences simultaneously [22,25,26]. The major limitation of this method is the presence of the fluorophore itself, as the large, charged fluorophore at the oligonucleotide's extremity has been shown to affect the surface coverage of DNA on AuNPs [25]. To quantify *unlabeled* DNA on AuNP, the DNA concentration in the supernatant before and after conjugation are measured using UV–vis spectroscopy [23,24]. This indirect method is simple and time-efficient but requires large amounts of DNA-AuNPs in order to have a measurable signal. Furthermore, this approach is also not suited to quantify multifunctional DNA-AuNPs. Multifunctional DNA-AuNPs are particularly interesting in biosensing assays where thiolated diluent DNA that act as spacers can be immobilized on AuNPs to alter the capture probe DNA density. In biological solutions where salt cations are present, DNA-AuNPs are susceptible to aggregation and coalescence as the electrostatic repulsion between the DNA strands decreases. Maintaining a certain total number of DNA on AuNPs is effective to prevent aggregation in salt solution. To improve the state-of-the-art of quantifying the surface density of DNA-AuNPs, we developed a rapid and reliable analytical method to quantify unlabeled DNA on AuNPs. In contrast to existing approaches, this method is also applicable for characterizing multifunctional DNA-AuNPs.

The working principle of the assay is to first release the immobilized DNA from the AuNP surface by dissolving the AuNPs with potassium cyanide (KCN), an efficient etchant for decomposition of AuNPs [15,24,27,28]. The released DNA strands are then hybridized with their complementary sequences (cDNA) and the double-stranded DNA (dsDNA) is stained with a dye for fluorescence readout (Fig. 1). Most DNA-AuNP applications prefer unlabeled DNA to be conjugated on AuNPs as the fluorescent DNA can alter the binding behavior of DNA-AuNPs to its potential target [24,25]. Traditionally, quantification with fluorescent DNA is performed routinely as a characterization for DNA-AuNPs but are then not used in the downstream applications. Such characterization inherently neglects the large batch-to-batch variation of DNA density on AuNPs which is critical for the reproducibility of a biosensing assay. Since our method requires less than 2 h, it can be easily implemented as a quality control for the DNA surface density prior to any DNA-AuNPs assay.

With this analytical quantification method, we evaluate several ways to precisely control the surface density of DNA-AuNPs: (1) Sodium chloride (NaCl) and initial DNA concentration during conjugation, (2) Displacing immobilized DNA with dithiothreitol (DTT), (3) Displacing immobilized DNA with excess backfilling thiolated DNA and (4) Exploiting the nature of the adenine (A) and thymine (T) spacers.

We observed that the achieved maximum DNA surface density on 50 nm AuNPs is about three times higher than what has previously been reported [22,29,30]. We also found that the saturation coverage of DNA-AuNPs can vary up to 30 % from batch to batch. These observations underline the need for a reliable analytical method that can assess the surface density of DNA on AuNPs precisely prior to using the conjugates in any application. For example, such a high level of control enabled us to optimize a miRNA sensing assay.

The stability of DNA-AuNPs is another major concern regarding their biomedical applications. In most cases, the main reason for the stability degradation of DNA-AuNPs is the non-stable thiol-gold bond which is affected by salt concentration [31], the pH level during storage [32], and temperature [33]. In most biological applications, salt cations are present which decrease the colloidal stability of DNA-AuNPs, causing non-specific DNA-medicated aggregation during the hybridization with the target of interest. This significantly affects the functional performance of the biosensor. We evaluated different DNA-AuNP storage conditions and found a solution for long-term storage by snap-freezing, which preserves the stability of DNA-AuNPs. This also helps further sensor optimization and it is a prerequisite for any future commercialization attempts.

2. Results and discussions

2.1. Assay principle

In order to quantify the average number of DNA molecules on a AuNP we need to measure the total number of AuNPs, their size distribution and the total amount of DNA bound to them. The number of AuNPs can be determined by absorbance spectroscopy as 50 nm AuNPs exhibit a characteristic absorbance peak at around 532 nm due to localized surface plasmon resonance [34,35]. Fig. 2**A** shows the normalized absorbance spectrum of different concentration of AuNPs from 0 to 75 pM indicating the characteristic absorbance peak at 532 nm with a dashed line. In our experiment, 75 pM is the stock concentration of AuNPs, hence the absorbance in Fig. 2**A** is presented as the normalized value to the stock concentration. The intensity of the absorbance peak is linearly dependent on the AuNP concentration, therefore, the number of AuNPs can be directly obtained from this calibration curve (Fig. 2B). Upon assumption that the colloids are perfectly monodispersed, the total surface area of gold in solution can be directly calculated from the number of AuNPs and the average AuNP diameter. However, during synthesis, the size and shape of AuNPs are influenced by sodium citrate concentration, stirring rate, temperature and production volume [36–38]. By simply taking the average diameter of AuNPs given by the manufacturer, the total AuNPs surface area can be underestimated depending on the AuNPs size distribution. Therefore, we used the measured effective diameter of the AuNPs in solution to calculate the total surface area of the AuNPs (Supporting Information **Fig. S1**). To determine the amount of DNA on the AuNPs, the AuNPs are first etched away and cDNA is added to form double stranded DNA (dsDNA). The sequence of this cDNA is chosen such that it is complementary to the DNA that we are interested in quantifying. After hybridization, a dsDNA dye (Quant-it™ PicoGreen™) is added to the DNA mixture, providing a fluorescent signal that corresponds to a given dsDNA concentration and consequently, to the amount of complementary single-stranded DNA (ssDNA) in the original solution.

In order to establish the relationship between the amount of dsDNA and the measured fluorescence, a calibration curve was recorded. Fig. 2**C** shows the linear correlation between the known amount of dsDNA and the fluorescence intensity of the dsDNA binding dye for the measured dsDNA concentrations which is well within range of the expected concentrations from the DNAs on AuNPs. The binding of PicoGreen to dsDNA has little sequence dependency [39], therefore, the

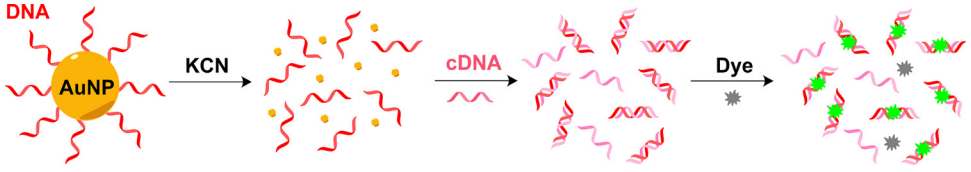

Fig. 1. Working principle of the quantification assay to assess the surface density of DNA-AuNPs. After cyanide (KCN) etching of the gold, the immobilized DNA is released from the AuNPs and hybridized with its complementary sequence. The resulting double-stranded DNA is stained specifically by dsDNA dye for quantification.

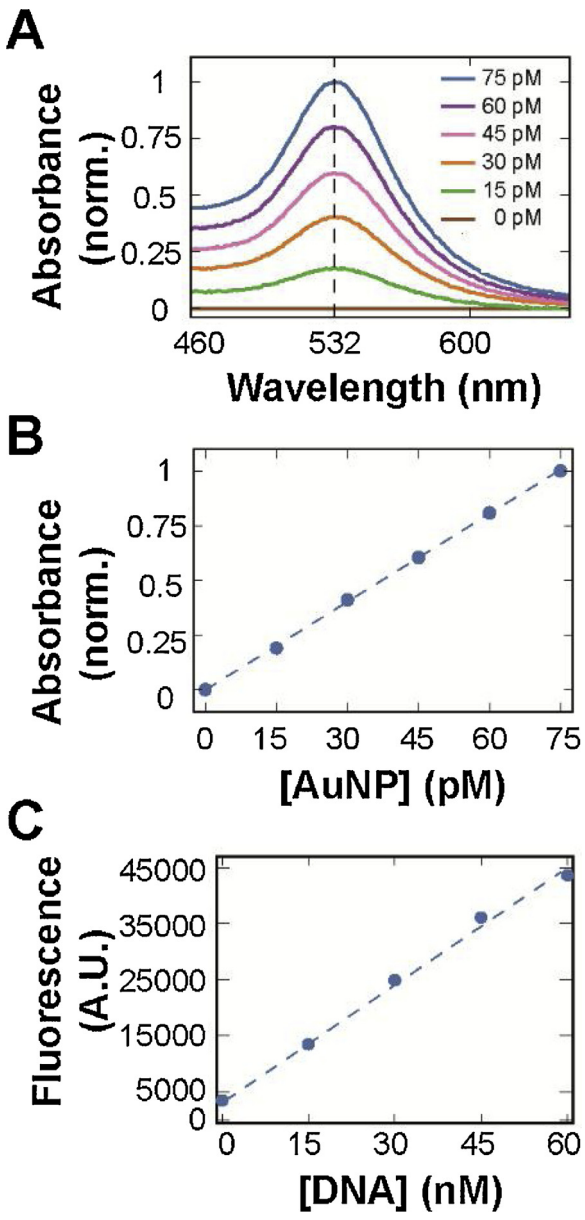

Fig. 2. A Normalized absorbance spectrum of AuNP solutions with concentration between 0–75 pM. **B** The intensity of the absorbance peak at 532 nm is linearly dependent of the AuNP concentration. Error bars indicating the standard deviation of six independent measurements are smaller than the symbol size. **C** Fluorescence signal as a function of dsDNA concentration. To ensure the fluorescent signal of the assay falls into the dynamic range of the dye, the range of DNA concentration of this calibration curve is chosen to include the dsDNA concentration expected from the maximal feasible surface density. The signal at 0 nM has an offset due to the presence of non-hybridized ssDNA in the solution. Error bars indicating the standard deviation of ten independent measurements are smaller than the symbol size.

calibration curve does not need to be repeated each time when performing the assay. The offset fluorescent signal at 0 nM dsDNA comes from ssDNA molecules in the solution, but it does not affect the linearity of the calibration curve in the assay (Supporting Information **Fig. S2**).

To avoid the potential signal contribution from free DNA in solution during conjugation, DNA-AuNPs undergo several washing rounds: Particles are centrifuged and the supernatant containing free DNA is removed and replaced by water or buffer (Supporting Information **Fig. S3**). The number of AuNP is determined before KCN etching of the particle. Etching is an important step of the assay as unetched AuNPs

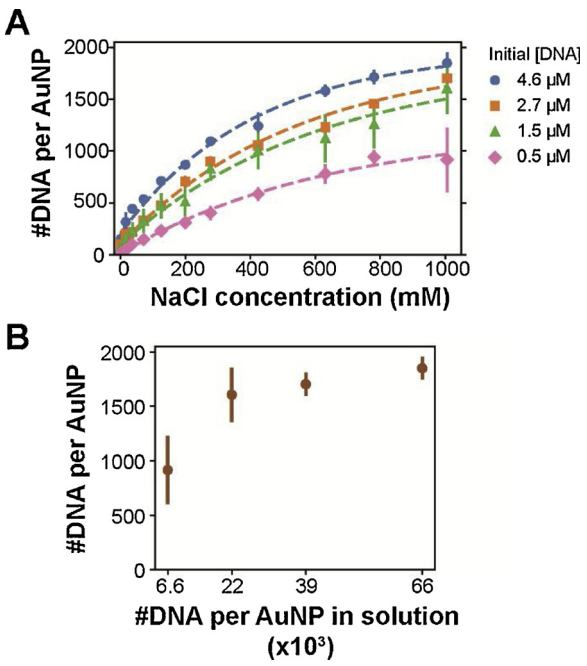

Fig. 3. A Wide range of surface densities of 50 nm DNA-AuNPs can be controlled by different NaCl and initial DNA concentration during conjugation. Error bars indicate the standard deviation of three independent measurements. **B** Maximal DNA strands per AuNP in function of DNA concentration in solution. Error bars indicate the standard deviation of three independent measurements.

could quench the fluorescent dye and lead to wrong results (Supporting Information **Fig. S4**) [15,24]. After 30 min, the completion of etching can be confirmed with absorbance measurements as the absorbance peak at 532 nm disappears (Supporting Information **Fig. S5**). For the KCN concentration used in this assay, no effect on DNA hybridization was observed (Supporting Information **Fig. S6**).

2.2. Controlling the surface density of DNA-AuNPs with NaCl and thiolated DNA during conjugation

As DNA density largely influences the binding efficiency of potential targets to DNA-AuNPs, having complete control over the surface density is essential for optimizing assay performance in different applications. Two of the most straightforward ways to control DNA surface density on AuNPs are: (1) controlling the final salt concentration (Fig. 3) and (2) changing the initial DNA concentration during DNA-AuNPs conjugation. [11,22]

We obtained AuNPs with a wide range of DNA densities by changing both salt and DNA concentrations (Fig. 3A). The DNA density increases with the DNA concentration during DNA-AuNPs conjugation, and a characteristic saturation curve is obtained when plotting the maximal density as a function of initial DNA concentration in solution (Fig. 3B). Here we also notice that denser particle DNA coverage can only be achieved by increasing the fold excess in the starting DNA concentration of the solution. While only about a 7-fold excess were needed to achieve close to 1000 DNA per particle, an over 30-fold excess was only sufficient to obtain less than 2000 DNA per particle indicating that we approached the expected saturation.

DNA coating is known to increase the stability of AuNP colloid suspensions because of the close range repulsive electrostatic interaction between the negatively charged DNA molecules [40]. However, this requires close to full coverage of the AuNPs to preserve the DNA-AuNPs' stability [41]. For applications that require different probe DNA densities, DNA spacers with no functional sequences or backfilling molecules such as DTT can be added onto the AuNPs' surface to increase the stability of DNA-AuNPs.

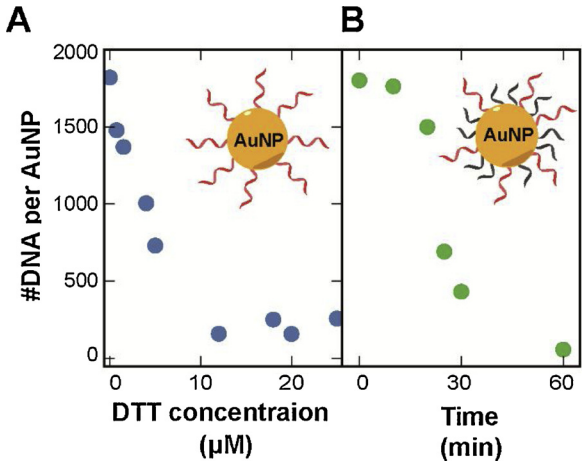

Fig. 4. A DTT displaces the immobilized DNA probes in a concentration-dependent manner. After 1 h of incubation with different concentrations of DTT, surface density of 50 nm DNA-AuNPs decreases. **B** Surface density of 50 nm DNA-AuNPs after 0 – 60 min of incubation with 10 μM of thiolated diluent DNA. By incubating excess thiolated diluent DNA with DNA-AuNPs, the diluent DNA displaces the immobilized DNA probes.

2.3. Controlling the surface density of DNA-AuNPs with DTT and thiolated diluent DNA

As we have shown above, although the surface density of DNA on AuNPs can be controlled by the concentration of NaCl and thiolated DNA during conjugation, this process requires the preparation of multiple batches of DNA-AuNPs under different conditions which is extremely time-consuming. DTT is a widely utilized reducing agent for separating thiolated ligands from gold surfaces [42,43]. By incubating DNA-AuNPs with different concentrations of DTT for 1 h, DTT displaces the immobilized probe DNA on AuNPs which enables the simultaneous preparation of particles with various surface densities as presented in Fig. 4**A**. At low probe density, however, the DNA-AuNPs are unstable as the total negative surface charge decreases drastically. To overcome the instability problem at low probe DNA density, thiolated diluent DNA that are not complimentary to the target molecule can be used as spacers. Displacement with diluent DNA ensures the overall total DNA number is high enough for the DNA-AuNPs to remain stable, while the probe DNA density can still be controlled (Fig. 4B). Since the quantification assay measures the dsDNA with high specificity, the amount of diluent DNA does not affect the assessment of the probe DNA density on the particle surface.

2.4. Controlling the surface density of DNA-AuNPs with spacer sequences

To render the probe DNA sequence on AuNPs more accessible for binding potential target DNA, a spacer sequence is often added to keep a distance between the probe DNA sequence and the AuNP surface. We investigated the effect of spacer composition on the surface density of DNA-AuNPs as it is known that the different deoxynucleotides, especially adenine (A) and thymine (T), possess different binding affinities to gold [15,19,28,41]. We assessed the surface density of DNA with two different spacers (polyA-DNA and polyT-DNA) (Fig. 5A), both DNAs are 22 bp long and apart from the 10 bp spacer, they have an identical recognition sequence (12 bp). While with the polyA spacer we found 1063 ± 293 DNA per 50 nm AuNP, when using the polyT spacer this number was substantially higher, *i.e.* 1808 ± 154 DNA per AuNP. If only consider the DNA geometry and neglect the electrostatic repulsion between the DNA strands, the density of a monolayer of DNA should be around 4000 DNAs per 50 nm AuNP. The difference in density suggests that the polyA tail adsorbs differently to a AuNP than the polyT tail (Fig. 5). The thiol functionalized ends form a covalent bond with the

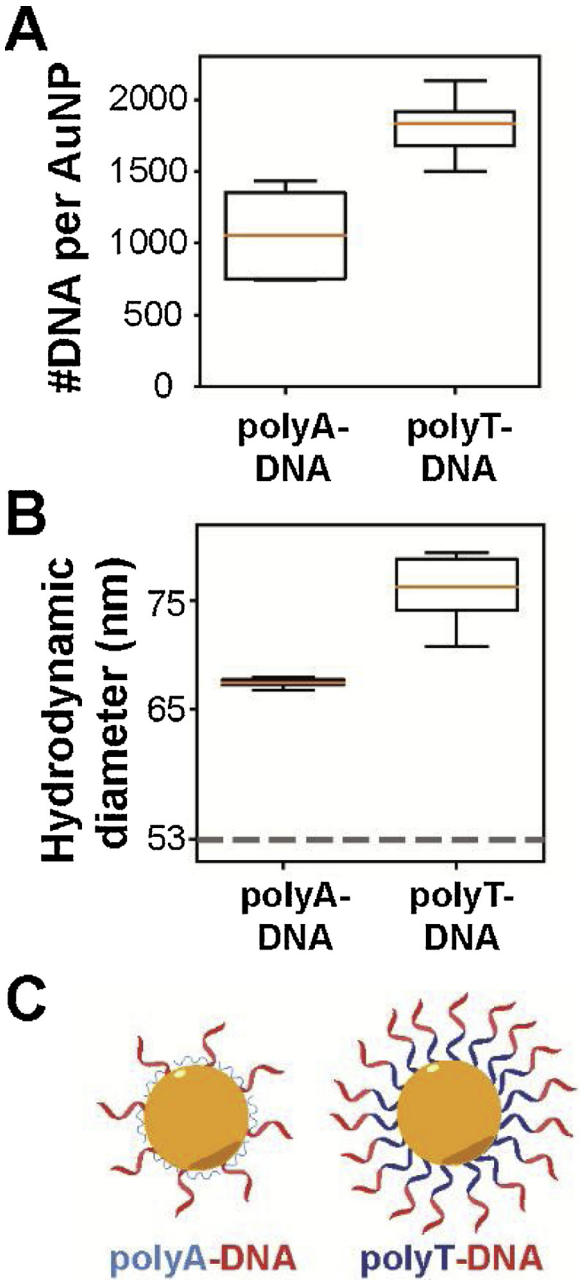

Fig. 5. A Loading of DNA with polyA and polyT spacer on 50 nm AuNP. Error bars indicate the standard deviation of twelve independent measurements. **B** Hydrodynamic diameter of DNA-AuNP with polyA and polyT spacer. PolyA spacers lead to a significantly reduced number of DNA strands per particle and a 10 nm thinner DNA layer around the particles. Gray dashed line at 53 nm indicates the hydrodynamic diameter of non-functionalized AuNPs. Error bars indicate the standard deviation of twelve independent measurements. **C** Hypothesized conformation of DNA with polyA and polyT spacers on AuNPs (not to scale). As reported in literature [15,22,41], DNA with polyA spacer has higher affinity to Au and lies flat on the AuNPs while polyT spacer interacts less with Au thus keeping the DNA in an upright conformation.

gold surface, but while the polyA spacer lies flat on the gold surface, the polyT spacer interacts less with the gold [15,19,28,41]. This concept depicted on Fig. 5**C** is further confirmed by the measured significantly smaller hydrodynamic size for the polyA tail DNA-AuNPs: 67.4 ± 0.4 nm for polyA-DNA AuNPs and 75.9 ± 2.9 nm for polyT-DNA AuNPs (Fig. 5B), indicating that the footprint of the polyA-DNA strand on the nanoparticle surface is considerably larger. The non-specific and non-covalent adsorption of the polyA spacer tail on the

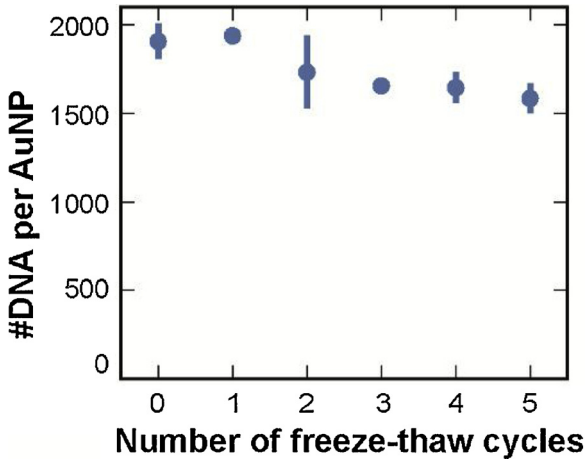

Fig. 6. Surface density of DNA-AuNPs after several freeze-thaw cycles in water with 20 % glycerol. After one freeze-thaw cycle, the amount of DNA on the AuNPs did not significantly decrease, demonstrating the possibility to snap freeze DNA-AuNPs for long term storage. Error bars indicate the standard deviation of three independent measurements.

AuNPs surface can alter the surface density but it is not always favorable for the hybridization of DNA-AuNPs with the target sequence. In addition, depending on the condition of the biosensing application, the conformation of the polyA-DNA can vary which introduces instability to the biosensing assay [44]. Therefore, polyT-DNA was chosen as the optimal spacer in the subsequent experiments.

2.5. Long-term storage of DNA-AuNPs

The conjugation of DNA-AuNPs is time consuming and their stability fluctuates greatly with storage conditions (Supporting Information **Fig. S7**) [32]. Therefore, storing DNA-AuNPs by snap freezing is the most useful condition to ensure the DNA-AuNPs remains stable, as the they can be prepared in larger quantity and be stored until usage. To assess the effect of freeze-thaw cycles on the DNA density on AuNPs, we conducted a series of snap freeze-thaw cycles on DNA-AuNPs. No significant decrease in the surface density of DNA after the first freezing was found. In fact, the surface density only decreased by 10 % after the second freeze-thaw cycle and remained stable even after 5 cycles (Fig. 6). This slight decrease in density after 5 cycles demonstrated the robustness of the DNA-AuNPs. Ideally for biosensing application, the DNA-AuNPs should be aliquoted into small volume and use it in one-go to avoid freezing the thawed DNA-AuNPs. Long term storage by snap freezing, together with our quantification method can be the solution to the current bottleneck of DNA-AuNPs commercialization. Both DNAs and AuNPs have reached industrial production scale, but currently laboratories working with DNA-AuNPs still rely on in-house conjugation facing reproducibility and DNA-AuNP instability issues. Implementing our quantification method as a quality control and storing DNA-AuNPs in a frozen state minimizes laborious conjugation processes and enhances the reproducibility of any DNA-AuNP-based assay.

2.6. Effect of surface density on miRNA sensing assay

50 nm AuNPs scatter light in green, while upon aggregation, their scattering peak intensity shifts towards longer wavelengths, also known as “red shifting” (Fig. 7A) [45]. We implemented a DNA-AuNP assay that uses this effect to distinguish between single and agglomerated AuNPs. The assay consisted of two batches of 50 nm AuNPs functionalized with two different probe DNAs. The two probe sequences (5′ thiol-DNA1 and 3′ thiol-DNA2, see Methods) were chosen to be complementary to the two halves of a target miRNA. In the absence of the target, both DNA-AuNPs stay as single particles with 50 nm average size

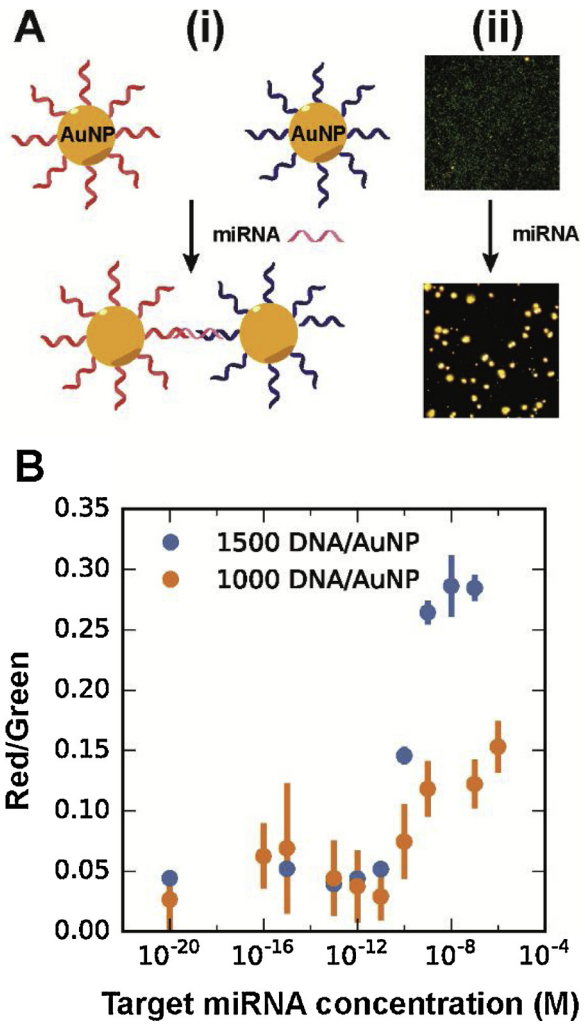

Fig. 7. A(i) Scheme of the miRNA target-mediated DNA-AuNP assay. In the presence of the miRNA (pink), two probe DNAs (red and blue) each hybridizes to half of the miRNA and result in particle aggregation. **A(ii)** Dark-field images of the DNA-AuNP assay. Single 50 nm DNA-AuNPs scatter green light which can be seen with a dark-field microscope (top image). Upon miRNA binding, DNA-AuNPs agglomerate and the scattered light shifts towards red (bottom image). **B** Dose-response of miRNA target-mediated DNA-AuNP assay with different surface probe DNA density. Low surface density (1000 DNA per AuNP in orange) results in unstable DNA-AuNPs and higher variation within a measurement. In the case of 1500 DNA per AuNP, the stability of DNA-AuNPs and the total signal of the dose response curve are both improved. Error bars indicate the standard deviation of three independent measurements (For interpretation of the references to colour in this figure legend, the reader is referred to the web version of this article.).

and consequently have a scattering peak intensity at 532 nm. Upon adding the target, pairs of the two differently functionalized particles are formed because the hybridized target molecules link them together. As such, the number of single DNA-AuNPs’ is reduced and a red shift in the scattering spectrum can be observed under a dark-field microscope (Fig. 7A). By measuring the scattering intensity of DNA-AuNPs at two different wavelengths (red and green), we can measure the level of agglomeration of the assay. Since the amount of miRNA in solution is proportional to the red shift caused by AuNP agglomeration, the red to green ratio of each dark-field microscope image is a measure of the target miRNA concentration [46].

With our quantification method, we evaluated the dose-response curve of DNA-AuNPs with 1500 DNA per AuNP and 1000 DNA per AuNP. As expected, the probe DNA surface density affects the performance of the assay (Fig. 7B). A low surface DNA density results in

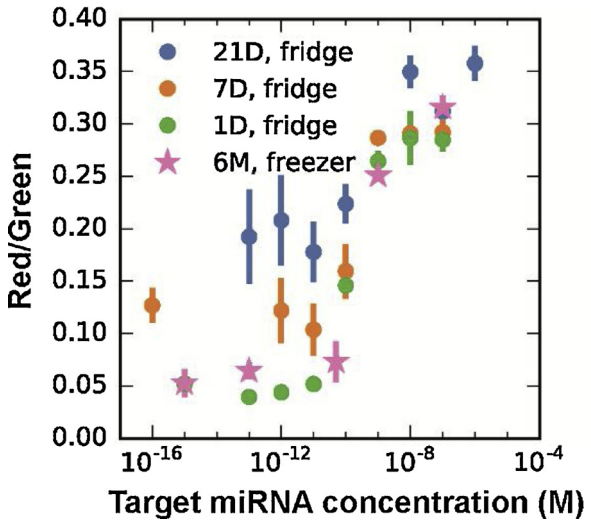

Fig. 8. Effect of storage time on the dose-response of miRNA target-mediated DNA-AuNP assay. The conjugated particles are stored in water at 4 °C and the assay is performed after 1, 7, and 21 days (there date points are shown in green, orange and blue circles). 1 day after the conjugation, the assay's limit of detection is 0.1 nM and in the mM range after 21 days of storage. Assay is also performed using long-term stored DNA-AuNPs. After 6 months of storage (pink star), the assay's performance is similar to the one of freshly prepared DNA-AuNPs. The limit of detection for the DNA-AuNPs stored after 6 months in the freezer is also 0.1 nM, demonstrating the long-term storing ability of the snap-freezing method. Error bars indicate the standard deviation of three independent measurements (For interpretation of the references to colour in this figure legend, the reader is referred to the web version of this article.).

unstable DNA-AuNPs which leads to partial and uncontrollable agglomeration of the particles which manifests as high error within a measurement. Higher surface DNA density not only improves the stability of DNA-AuNP but also increases the signal and improves the reproducibility of the assay.

2.7. Effect of DNA-AuNPs' stability on miRNA sensing assay

Using the same DNA-AuNP assay for miRNA sensing, we demonstrated how the long-term storage is crucial for a well-controlled sensor. DNA-AuNPs after conjugation are commonly stored in solution at 4 °C or 25 °C in different buffer conditions. We have found that the particles aggregate with time when stored in buffer solution (Supporting Information **Fig. S7**) and the limit of detection of the assay is worsened from sub-nM to mM (Fig. 8). At low target concentration, older DNA-AuNPs showed higher red over green signal. This is due to the non-specific aggregation and sedimentation of the particles, which also has a strong negative effect on the assay performance. This highlights the susceptibility of DNA-AuNPs' stability to storage time. As the preparation of DNA-AuNPs is tedious, it often takes more than 12 h, the solution of long-term storage of DNA-AuNPs will effectively decrease the preparation time and ensure the quality of the particles.

3. Conclusions and outlook

We showed a simple analytical method for the quantification of multiple unlabeled oligonucleotides on AuNPs. With the help of this quantification method, we demonstrated how to control DNA density on DNA-AuNPs for biosensing applications.

DNA loading depends on many factors: the quality of DNA from the manufacturer, salt concentration, initial DNA concentration, orientation, DNA sequence and length, as well as the size of the particle. However, with our method, DNA-AuNPs can be better characterized, and the precise DNA surface density can be obtained. Previous methods based on fluorescently-labeled DNA are based on the assumption that the coverage does not differ drastically to the one of unlabeled DNA. Here, we demonstrated about 3 times higher DNA densities than what has been previously reported by other quantification methods. We believe that the absence of a fluorophore during conjugation might be the explanation for this substantial increase. As DNA density on AuNPs can vary for different conditions and application requirements, having a fast and reliable quantification method can minimize the reproducibility problems of DNA-AuNP conjugation.

To ensure the stability of DNA-AuNPs during storage, we proposed a long-term storage method by snap freezing. This eliminates the need to repeat the time-consuming and laborious DNA-AuNP preparation over and over again before each experiment while guaranteeing the stability of the conjugated particles. This drastically improves reproducibility and as such it is highly beneficial to any DNA-AuNP-based applications.

As an example, we showed the importance of using well-controlled and characterized DNA-AuNPs to assure good performance for a biosensors application. Here, we took miRNA as a target for our DNA-AuNP assay. miRNA are considered important biomarkers for numerous diseases, notably cancer, as aberrant miRNA expression is found to correlate with disease type and stage. We showed that the probe DNA density on AuNPs effects the dose-response curve of the assay. We also showed that with the traditional storage conditions for DNA-AuNPs, the limit of detection of the sensor went from sub-nM to mM after only 21 days illustrating the importance of our long-term storage solution.

The use of DNA as receptors is not limited to hybridization based sensing. It can also be applied to aptamers, i.e. short nucleic acid sequences with antibody-like specificity towards a given analyte that can be engineered for ion sensing [47], drug delivery [48] and cancerous cell detection [49]. Our quantification assay and storage solution can also be beneficial to assess the surface density of aptamers on AuNPs, benefiting biosensors with even broader applications [50,51].

4. Materials and methods

4.1. Materials

50 nm citrate capped AuNPs were purchased from BBI Solutions. DNA sequences (Table 1) were custom-synthesized and purified (HPLC) by Microsynth AG. Quant-it™ PicoGreen™ dsDNA Assay was purchased from Thermo Fisher Scientific. Tris (2-carboxyethyl) phosphine (TCEP), sodium dodecyl sulfate (SDS), phosphate buffered saline (PBS), potassium cyanide (KCN) and sodium chloride (NaCl) were purchased from Sigma-Aldrich. All aqueous solutions were prepared using purified Milli-Q water from an Elix 5 water purification system (Merck Millipore). All buffers were filtered with Minisart 0.2 µm filters from Sigma Aldrich. 96 well microplates for fluorescence readout (PS, F-bottom, black) were purchased from Greiner Bio-One. 96 well microplates for absorbance measurement (TPP, F-bottom, transparent) were purchased from TPP. 8-well 0.2 ml PCR tube strips were purchased from Thermo Fisher Scientific. Cuvettes for DLS measurements were purchased from Malvern Panalytical.

Table 1
Nomenclature and sequence of the used DNA and RNA.

DNA name	Sequence (5′ – 3′)
5′ thiol-DNA1	TTTTTTTTTTCGCATTCAGGAT
cDNA1	ATCCTGAATGCGAAAAAAAAAA
5′ thiol-diluent DNA	GGGGGGGGGG
3′ thiol-diluent DNA	GGGGGGGGGG
polyA-DNA	TCTCAACTCGTAAAAAAAAAAA
polyT-DNA	TCTCAACTCGTATTTTTTTTTT
3′ thiol-DNA2	TCTCAACTCGTATTTTTTTTTT
cDNA2	AAAAAAAAAATACGAGTTGAGA
Target miRNA	UACGAGUUGAGAAUCCUGAAUGCG

4.2. Preparation of DNA-AuNPs conjugates

The conjugated DNA-AuNPs were synthesized using a modified literature protocol [19]. Thiolated oligonucleotides were reduced at room temperature with excess TCEP for 1 h. AuNPs were mixed with the reduced DNA and 0.02 % SDS final concentration. For the standard conjugation protocol, 4.6 μM of reduced DNA was added to 500 μl of stock AuNPs which corresponds to a DNA:AuNP ratio of 62,000:1. When investigating the effect of DNA concentrations during conjugation on the final DNA surface density on AuNPs, the DNA concentration was modified to 2.7, 1.5, and 0.5 μM. After an overnight incubation, 2 M NaCl and 100 mM PBS were incrementally added to reach final concentration of 1 M NaCl and 10 mM PBS, while sonicating briefly after each salt addition step to prevent agglomeration. The samples were incubated overnight in the final salt solution at room temperature, then centrifuged for 5 min at 14,100 *g* before washing with Milli-Q water to remove excess free DNA. After three washing rounds the particles were resuspended in 10 mM PSB. For conjugation of different DNA sequences on AuNPs, the DNA1 and DNA2 were mixed as different ratios while keeping the total amount of DNA constant.

4.3. Long-term storage for DNA-AuNPs

DNA-AuNPs after conjugation were suspended in water with 20 % glycerol. DNA-AuNPs of 3×10^{10}cAuNP/ml were prepared into 10 μl aliquots and snap-froze in liquid nitrogen for 10 s. The frozen aliquots were then stored in -80 °C for long-term storage.

4.4. Quantification assay for DNA-AuNPs

The calibration curve of the assay is composed of 0, 15, 30, 45 and 60 nM of ssDNA which were mixed with 50 pM of bare AuNPs resuspended in 10 mM PBS (Fig. 2C). The bare AuNPs aggregate in PBS, however, theses samples are prepared for the calibration curve and therefore the stability of the AuNPs are not a concern. During the etching process, the formation of the soluble cyano-complex $Au(CN)_2$ can affect the read-out fluorescent signal. Therefore, to ensure the sample prepared for the calibration curve is identical as the measured sample, the calibration curve was established with known concentration of ssDNA and bare AuNPs. Absorbance spectra of AuNPs were taken prior to AuNP etching at a final concentration of 5 mM KCN. To avoid diluting the ssDNA in the assay, small volume of a highly concentrated stock solution was used. After 30 min of etching, the initially pink solution turned transparent which confirmed the completion of AuNP etching (Supporting Information **Fig. S8**). 60 μl of conjugated DNA-AuNPs ($\sim 3 \times 10^{10}$AuNP/ml) were added in 40 μl of PBS and etched in the same conditions as the calibration samples. After etching, the DNA attached on AuNP is released. The KCN solution and buffers were kept at room temperature and regularly renewed. All samples were hybridized with 60 nM of cDNA. The samples were heated up and kept at 45 °C for 10 min before cooling down to room temperature for hybridization. This temperature is unusually low for DNA hybridization compared to standard polymerase chain reaction protocols. It was chosen to exceed the melting temperature of undesired DNA duplexes, while being low enough to limit the acceleration of cyanide hydrolysis and subsequent release of toxic hydrogen cyanide gas (Supporting Information **Fig. S6**). After hybridization, 100 μl of the sample solution was transferred to a 96 black-bottomed well-plate. 100 μl of freshly prepared dye solution according to the manufacturer instruction was added to each well. The calibration curve was fitted with a linear function ($y = 0.013x - 0.001$) and used to determine the amount of DNA in the sample solution. The concentration of DNA in the well was determined by reading the calibration curve.

4.5. Quantification assay for dual-functionalized AuNPs

As the total surface density can vary from experiment to experiment, in dual-functionalized quantification assay, both the total surface density and the ratio of the two DNAs are unknown. Therefore, a 2-parameters calibration curve was prepared, varying both the total DNA concentration and the ratio between the two DNAs (**Fig. S9**). All samples were adjusted to the same AuNP concentration (3×10^{10} AuNP/ml) prior to analysis. Solution containing different total DNA concentration and different ratio of DNA1 to DNA2 were split into two, and one was analyzed with cDNA1 and the other with cDNA2 (Supporting Information **Fig. S9**). Experimental procedures were identical to those used for the characterization mono-functionalized DNA-AuNPs, except that each dual sample was separated into two equal portions prior to cDNA addition, and then each obtained portion was mixed with the respective cDNA for its hybridization.

4.6. DTT and thiolated diluent DNA treatment for controlling the surface density of DNA-AuNPs

DNA-AuNPs with maximal surface density (~1800 DNA per AuNP) were incubated at different DTT concentration (0–25 μM) for 1 h. The particles were then centrifuged for 5 min at 14,100 g before washing with Milli-Q water to remove the displaced DNA as well as the free DTT in solution. The quantification assay was performed as previously described to obtain the average number of DNA per AuNP after DTT treatment. The same assay was used to evaluate the displacement of immobilized probe DNA with thiolated diluent DNA. DNA-AuNPs with maximal surface density (~1800 DNA per AuNP) were incubated with 10 μM of thiolated diluent DNA for 0 − 60 min. The diluent DNA was a short, 10 base pair long polyG DNA (Table 1) and the purpose of these diluent DNA was to act as spacers to control the surface density of probe DNA on AuNPs, while preserving the total number of DNA constant in order to maintain the stability of the particle solution.

4.7. miRNA sensing assay with DNA-AuNPs

In order to visualize the particle aggregation upon target hybridization, dark-field images were collected using a dark-field microscope. AuNP assay was prepared by mixing 1 part of AuNPs (4.5×10^9 particles/ml) functionalized with 5′ thiol-DNA1; 1 part of AuNPs functionalized with 3′ thiol-DNA2; which were mixed with 2 parts of the target miRNA in PBS. The AuNP assay underwent a heat cycle of 10 min at 75 °C and 2 h at 25 °C with commercial thermocycler (Biometra T-Personal Combi Thermocycler, Biometra GmbH). 10 μl of AuNP assay with the desired target concentration was loaded in customized polydimethylsiloxane (PDMS) wells on microscopy slides. Microscopy slides and cover slips (Menzel-Gläser, Gerhard Menzel-Gläser GmbH) were cleaned by submersing the glass slides in Hellmanex III 2 % and ultrasonicated for 5 min. The glass slides were then cleaned in water bath and ultrasonicated for 5 min. Nitrogen stream was used to dry the cleaned glass slides. Polydimethylsiloxane (PDMS) sheets of 5 mm thickness were cut to size and 2 mm wells were stamped out with a biopsy punch. The PDMS wells were covered with a cover slip after the sample solutions were added. The AuNPs require sedimentation on the microscopy slide to be imaged with a dark-field microscope. To achieve this, the samples were left overnight for particle settling. On the following day, cover slips and PDMS wells were carefully removed and new cover slips were added. A hyperspectral nanoscale optical imaging system consisting of an Olympus BX53 F microscope, an enhanced dark-field optical illumination system (CytoViva Inc.), an objective (Olympus UPlanFLN 60x/1.25 Oil Iris) and a CMOS camera was used for image acquisition in transmission mode. The images were analyzed with a customized Python script. First, the images were normalized and Gaussian blurred with a standard deviation of 2 pixels. Afterwards, the script detects the maxima of the sum of

green and red intensities of the images. A maximum was determined as the center of a particle if two conditions were fulfilled: (1) the maximum is the highest value in its vicinity (3 pixels) and (2) the maximum is above a threshold of 0.03. Once the center of the particle is located, a mean radial profile of the summed up intensity map was generated for each particle in order to estimate the particle size. The particles were assumed spherical and the radius of the particle was determined by the distance from the center of the particle to the closest minimum. The radius was upper bounded at 35 pixels as no particle bigger than this size was observed. Finally, the red and green intensities of a particle were calculated by integrating the normalized intensity over the particle size of the blurred red and green channel, respectively.

CRediT authorship contribution statement

Stephanie Hwu: Conceptualization, Methodology, Software, Validation, Formal analysis, Investigation, Data curation, Writing - original draft, Writing - review & editing, Visualization, Supervision. **Manon Garzuel:** Methodology, Software, Validation, Formal analysis, Investigation, Data curation, Writing - original draft, Writing - review & editing, Visualization. **Csaba Forró:** Methodology, Software, Formal analysis, Data curation, Writing - review & editing, Visualization. **Stephan J. Ihle:** Methodology, Software, Formal analysis, Data curation, Writing - review & editing. **Andreas M. Reichmuth:** Writing - review & editing. **Fiodar Kurdzesau:** Methodology, Investigation, Writing - review & editing. **János Vörös:** Conceptualization, Writing - review & editing, Supervision, Funding acquisition.

Declaration of Competing Interest

The authors declare no competing financial interests.

Acknowledgments

The work was supported by the Swiss National Foundation (Switzerland) and ETH Zurich (Switzerland). We thank Dr. Nako Nakatsuka for giving feedback on the manuscript. We also thank Prof. Dr. Raffaele Mezzenga, Yiping Cao, Mattia Usuelli from the Department of Health Sciences and Technology at ETH Zurich for the access to Zetasizer, and Prof. Dr. Samuel C. Zeeman and Dr. Laure David from the Department of Biology at ETH Zurich for the access to Tecan Plate Reader.

Appendix A. Supplementary data

Supplementary material related to this article can be found, in the online version, at doi:https://doi.org/10.1016/j.colsurfb.2019.110650.

References

[1] J.-M. Nam, C.S. Thaxton, C.A. Mirkin, Nanoparticle-based bio-bar codes for the ultrasensitive detection of proteins, Science 301 (5641) (2003) 1884–1886, https://doi.org/10.1126/science.1088755.
[2] K. Saha, S.S. Agasti, C. Kim, X. Li, V.M. Rotello, Gold nanoparticles in chemical and biological sensing, Chem. Rev. 112 (5) (2012) 2739–2779, https://doi.org/10.1021/cr2001178.
[3] C.-C. Chien, H.-H. Chen, S.-F. Lai, K.-C. Wu, X. Cai, Y. Hwu, C. Petibois, Y. Chu, G. Margaritondo, Gold nanoparticles as high-resolution X-Ray imaging contrast agents for the analysis of tumor-related micro-vasculature, J. Nanobiotechnology 10 (1) (2012) 10, https://doi.org/10.1186/1477-3155-10-10.
[4] M. Boksebeld, V. Kilin, R. Taitt, L. Bonacina, A. Géloën, V. Lysenko, Y. Chevolot, V. Monnier, Nonlinear plasmonic nanohybrids as probes for multimodal cell imaging and potential phototherapeutic agents, Biomed. Phys. Eng. Express 5 (2) (2019) 025039, , https://doi.org/10.1088/2057-1976/ab0232.
[5] E. Blanco, H. Shen, M. Ferrari, Principles of nanoparticle design for overcoming biological barriers to drug delivery, Nat. Biotechnol. 33 (9) (2015) 941–951, https://doi.org/10.1038/nbt.3330.
[6] C.-H. Chu, Y.-C. Wang, L.-A. Tai, L.-C. Wu, C.-S. Yang, Surface deformation of gold nanorod -Loaded poly(dl -Lactide- Co -Glycolide) nanoparticles after near infrared irradiation: an active and controllable drug release system, J. Mater. Chem. 20 (16) (2010) 3260–3264, https://doi.org/10.1039/B925651M.
[7] N.L. Rosi, C.A. Mirkin, Nanostructures in Biodiagnostics, Chem. Rev. 105 (4) (2005) 1547–1562, https://doi.org/10.1021/cr030067f.
[8] D.A. Giljohann, C.A. Mirkin, Drivers of biodiagnostic development, Nature 462 (7272) (2009) 461–464, https://doi.org/10.1038/nature08605.
[9] H. Schwarzenbach, D.S.B. Hoon, K. Pantel, Cell-free nucleic acids as biomarkers in cancer patients, Nat. Rev. Cancer 11 (6) (2011) 426–437, https://doi.org/10.1038/nrc3066.
[10] D.P. Bartel, MicroRNAs: genomics, biogenesis, mechanism, and function, Cell 116 (2) (2004) 281–297, https://doi.org/10.1016/S0092-8674(04)00045-5.
[11] J.J. Storhoff, R. Elghanian, R.C. Mucic, C.A. Mirkin, R.L. Letsinger, One-pot colorimetric differentiation of Polynucleotides with single base imperfections using gold nanoparticle probes, J. Am. Chem. Soc. 120 (9) (1998) 1959–1964, https://doi.org/10.1021/ja972332i.
[12] R.A. Reynolds, C.A. Mirkin, R.L. Letsinger, Homogeneous, Nanoparticle-Based Quantitative Colorimetric Detection of Oligonucleotides, J. Am. Chem. Soc. 122 (15) (2000) 3795–3796, https://doi.org/10.1021/ja000133k.
[13] A.K.R. Lytton-Jean, C.A. Mirkin, A thermodynamic investigation into the binding properties of DNA functionalized gold nanoparticle probes and molecular fluorophore probes, J. Am. Chem. Soc. 127 (37) (2005) 12754–12755, https://doi.org/10.1021/ja052255o.
[14] D.A. Giljohann, D.S. Seferos, P.C. Patel, J.E. Millstone, N.L. Rosi, C.A. Mirkin, Oligonucleotide loading determines cellular uptake of DNA-Modified gold nanoparticles, Nano Lett. 7 (12) (2007) 3818–3821, https://doi.org/10.1021/nl072471q.
[15] L.M. Demers, C.A. Mirkin, R.C. Mucic, R.A. Reynolds, R.L. Letsinger, R. Elghanian, G. Viswanadham, A fluorescence-based method for determining the surface coverage and hybridization efficiency of thiol-capped oligonucleotides bound to gold thin films and nanoparticles, Anal. Chem. 72 (22) (2000) 5535–5541, https://doi.org/10.1021/ac0006627.
[16] K.A. Brown, S. Park, K. Hamad-Schifferli, Nucleotide − Surface interactions in DNA-Modified Au − Nanoparticle conjugates: sequence effects on reactivity and hybridization, J. Phys. Chem. C 112 (20) (2008) 7517–7521, https://doi.org/10.1021/jp711869p.
[17] B. Liu, J. Liu, Methods for preparing DNA-Functionalized gold nanoparticles, a key reagent of bioanalytical chemistry, Anal. Methods 9 (18) (2017) 2633–2643, https://doi.org/10.1039/C7AY00368D.
[18] M.F. Hagan, A.K. Chakraborty, Hybridization dynamics of surface immobilized DNA, J. Chem. Phys. 120 (10) (2004) 4958–4968, https://doi.org/10.1063/1.1645786.
[19] C.A. Mirkin, R.L. Letsinger, R.C. Mucic, J.J. Storhoff, A DNA-Based method for rationally assembling nanoparticles into macroscopic materials, Nature 382 (6592) (1996) 607–609, https://doi.org/10.1038/382607a0.
[20] X. Zhang, M.R. Servos, J. Liu, Instantaneous and quantitative functionalization of gold nanoparticles with thiolated DNA using a PH-Assisted and surfactant-free route, J. Am. Chem. Soc. 134 (17) (2012) 7266–7269, https://doi.org/10.1021/ja3014055.
[21] H. Yu, X. Xu, P. Liang, K.Y. Loh, B. Guntupalli, D. Roncancio, Y. Xiao, A broadly applicable assay for rapidly and accurately quantifying DNA surface coverage on diverse particles, Bioconjug. Chem. 28 (4) (2017) 933–943, https://doi.org/10.1021/acs.bioconjchem.6b00660.
[22] S.J. Hurst, A.K.R. Lytton-Jean, C.A. Mirkin, Maximizing DNA loading on a range of gold nanoparticle sizes, Anal. Chem. 78 (24) (2006) 8313–8318, https://doi.org/10.1021/ac0613582.
[23] Q. Xu, X. Lou, L. Wang, X. Ding, H. Yu, Y. Xiao, Rapid, Surfactant-Free, and Quantitative Functionalization of Gold Nanoparticles with Thiolated DNA under Physiological PH and Its Application in Molecular Beacon-Based Biosensor, ACS Appl. Mater. Interfaces 8 (40) (2016) 27298–27304, https://doi.org/10.1021/acsami.6b08350.
[24] B.L. Baldock, J.E. Hutchison, UV–Visible spectroscopy-based quantification of unlabeled DNA bound to gold nanoparticles, Anal. Chem. 88 (24) (2016) 12072–12080, https://doi.org/10.1021/acs.analchem.6b02640.
[25] R.E. Paliwoda, F. Li, M.S. Reid, Y. Lin, X.C. Le, Sequential strand displacement beacon for detection of DNA coverage on functionalized gold nanoparticles, Anal. Chem. 86 (12) (2014) 6138–6143, https://doi.org/10.1021/ac501341t.
[26] R.J. Stokes, A. Macaskill, P.J. Lundahl, W.E. Smith, K. Faulds, D. Graham, Quantitative enhanced raman scattering of labeled DNA from gold and silver nanoparticles, Small 3 (9) (2007) 1593–1601, https://doi.org/10.1002/smll.200600662.
[27] J.I. Cutler, K. Zhang, D. Zheng, E. Auyeung, A.E. Prigodich, C.A. Mirkin, Polyvalent nucleic acid nanostructures, J. Am. Chem. Soc. 133 (24) (2011) 9254–9257, https://doi.org/10.1021/ja203375n.
[28] X. Zhang, B. Liu, M.R. Servos, J. Liu, Polarity control for nonthiolated DNA adsorption onto gold nanoparticles, Langmuir 29 (20) (2013) 6091–6098, https://doi.org/10.1021/la400617u.
[29] H.D. Hill, J.E. Millstone, M.J. Banholzer, C.A. Mirkin, The role radius of curvature plays in thiolated oligonucleotide loading on gold nanoparticles, ACS Nano 3 (2) (2009) 418–424, https://doi.org/10.1021/nn800726e.
[30] X. Zhang, T. Gouriye, K. Göeken, M.R. Servos, R. Gill, J. Liu, Toward fast and quantitative modification of large gold nanoparticles by thiolated DNA: scaling of nanoscale forces, kinetics, and the need for thiol reduction, J. Phys. Chem. C 117 (30) (2013) 15677–15684, https://doi.org/10.1021/jp403946x.
[31] R. Pamies, J.G.H. Cifre, V.F. Espín, M. Collado-González, F.G.D. Baños, J.G. de la Torre, Aggregation behaviour of gold nanoparticles in saline aqueous media, J. Nanopart. Res. 16 (4) (2014), https://doi.org/10.1007/s11051-014-2376-4.
[32] N. Bhatt, P.-J.J. Huang, N. Dave, J. Liu, Dissociation and degradation of thiol-

modified DNA on gold nanoparticles in aqueous and organic solvents, Langmuir 27 (10) (2011) 6132–6137, https://doi.org/10.1021/la200241d.
[33] F. Li, H. Zhang, B. Dever, X.-F. Li, X.C. Le, Thermal stability of DNA functionalized gold nanoparticles, Bioconjug. Chem. 24 (11) (2013) 1790–1797, https://doi.org/10.1021/bc300687z.
[34] W. Haiss, N.T.K. Thanh, J. Aveyard, D.G. Fernig, Determination of size and concentration of gold nanoparticles from UV-Vis spectra, Anal. Chem. 79 (11) (2007) 4215–4221, https://doi.org/10.1021/ac0702084.
[35] T. Sannomiya, J. Vörös, Single plasmonic nanoparticles for biosensing, Trends Biotechnol. 29 (7) (2011) 343–351, https://doi.org/10.1016/j.tibtech.2011.03.003.
[36] B.V. Enustun, John. Turkevich, Coagulation of colloidal gold, J. Am. Chem. Soc. 85 (21) (1963) 3317–3328, https://doi.org/10.1021/ja00904a001.
[37] G. Frens, Controlled nucleation for the regulation of the particle size in monodisperse gold suspensions, Nat. Phys. Sci. 241 (105) (1973) 20–22, https://doi.org/10.1038/physci241020a0.
[38] J. Kimling, M. Maier, B. Okenve, V. Kotaidis, H. Ballot, A. Plech, Turkevich method for gold nanoparticle synthesis revisited, J. Phys. Chem. B 110 (32) (2006) 15700–15707, https://doi.org/10.1021/jp061667w.
[39] A.I. Dragan, J.R. Casas-Finet, E.S. Bishop, R.J. Strouse, M.A. Schenerman, C.D. Geddes, Characterization of PicoGreen interaction with DsDNA and the origin of its fluorescence enhancement upon binding, Biophys. J. 99 (9) (2010) 3010–3019, https://doi.org/10.1016/j.bpj.2010.09.012.
[40] S.S. Hinman, K.S. McKeating, Q. Cheng, DNA linkers and diluents for ultrastable gold nanoparticle bioconjugates in multiplexed assay development, Anal. Chem. 89 (7) (2017) 4272–4279, https://doi.org/10.1021/acs.analchem.7b00341.
[41] J.J. Storhoff, R. Elghanian, C.A. Mirkin, R.L. Letsinger, Sequence-dependent stability of DNA-Modified gold nanoparticles, Langmuir 18 (17) (2002) 6666–6670, https://doi.org/10.1021/la0202428.
[42] D.-H. Tsai, T.J. Cho, F.W. DelRio, J.M. Gorham, J. Zheng, J. Tan, M.R. Zachariah, V.A. Hackley, Controlled formation and characterization of dithiothreitol-conjugated gold nanoparticle clusters, Langmuir 30 (12) (2014) 3397–3405, https://doi.org/10.1021/la500044y.
[43] P. Liang, J. Canoura, H. Yu, O. Alkhamis, Y. Xiao, Dithiothreitol-regulated coverage of oligonucleotide-modified gold nanoparticles to achieve optimized biosensor performance, ACS Appl. Mater. Interfaces 10 (4) (2018) 4233–4242, https://doi.org/10.1021/acsami.7b16914.
[44] X. Zhang, M.R. Servos, J. Liu, Surface science of DNA adsorption onto citrate-capped gold nanoparticles, Langmuir 28 (8) (2012) 3896–3902, https://doi.org/10.1021/la205036p.
[45] J.J. Storhoff, A.A. Lazarides, R.C. Mucic, C.A. Mirkin, R.L. Letsinger, G.C. Schatz, What controls the optical properties of DNA-Linked gold nanoparticle assemblies? J. Am. Chem. Soc. 122 (19) (2000) 4640–4650, https://doi.org/10.1021/ja993825l.
[46] P. Rajendran, S. Kaufmann, J. Vörös, M. Zenobi-Wong, L. Demkó, Femtomolar oligonucleotide detection by a one-step gold nanoparticle-based assay, Colloids Surf. B Biointerfaces 135 (2015) 193–200, https://doi.org/10.1016/j.colsurfb.2015.07.035.
[47] W. Zhao, W. Chiuman, J.C.F. Lam, S.A. McManus, W. Chen, Y. Cui, R. Pelton, M.A. Brook, Y. Li, DNA aptamer folding on gold nanoparticles: from colloid chemistry to biosensors, J. Am. Chem. Soc. 130 (11) (2008) 3610–3618, https://doi.org/10.1021/ja710241b.
[48] D. Kim, Y.Y. Jeong, S. Jon, A drug-loaded aptamer – Gold nanoparticle bioconjugate for combined CT imaging and therapy of prostate Cancer, ACS Nano 4 (7) (2010) 3689–3696, https://doi.org/10.1021/nn901877h.
[49] C.D. Medley, J.E. Smith, Z. Tang, Y. Wu, S. Bamrungsap, W. Tan, Gold nanoparticle-based colorimetric assay for the direct detection of cancerous cells, Anal. Chem. 80 (4) (2008) 1067–1072, https://doi.org/10.1021/ac702037y.
[50] Z. Zhang, Y. Liu, C. Jarreau, M.J. Welch, J.-S.A. Taylor, Nucleic acid-directed self-assembly of multifunctional gold nanoparticle imaging agents, Biomater. Sci. 1 (10) (2013) 1055–1064, https://doi.org/10.1039/C3BM60070J.
[51] Y. Hoon Roh, R.C. H. Ruiz, S. Peng, J. Bum Lee, D. Luo, Engineering DNA-Based functional materials, Chem. Soc. Rev. 40 (12) (2011) 5730–5744, https://doi.org/10.1039/C1CS15162B.